Real-Time Global Retrievals of Cloud Spatial, Radiative, and Microphysical Properties

Robert P. d'Entremont, Gary B. Gustafson, Jean-Luc Moncet and Alan Lipton
Atmospheric and Environmental Research, Inc.
Lexington, MA 02421-3126 USA

Abstract: Clouds have a strong influence on radiative forcing of the Earth-atmosphere-ocean system. Radiative energy fluxes drive the exchange of mass and energy between the Earth's land and ocean surfaces and the atmosphere. For example when the surface experiences a net gain of radiative energy then it is likely that any water will evaporate from the ground into the atmosphere, with corresponding exchanges of sensible and latent heat. The mechanisms that control how latent and sensible heats are partitioned are complex and depend on land-surface and atmospheric conditions alike. One thing is certain however: knowing the net gain/loss of radiative energy at the Earth's land surface is critical for prescribing these energy partitions. In a cloud-free atmosphere the shortwave and longwave fluxes are relatively straightforward to prescribe in comparison to cloudy atmospheres. With a wide variety of optical and radiative properties, as prescribed by the cloud-particle microphysics, their net effect in any region can be to warm or to cool the land surface. Cloud radiative properties also influence strongly atmospheric heating and cooling rates.

From a radiative-transfer modeling perspective the three main cloud properties that drive the land-surface, atmospheric, and top-of-atmosphere radiative flux balances are optical thickness, single scattering albedo, and asymmetry parameter. In turn these are prescribed for all wavelengths by the wavelength-independent cloud-particle size distribution (SD) and the morphology of the individual particles themselves. For example, the radiative attributes of round droplets differ considerably from those of irregularly shaped ice particles. For the former, the well established Mie theory is applicable; for the latter, we choose a measurements-based approximation to anomalous diffraction theory. Either way, the spectra of routinely available satellite-based passive radiance observations typically does not contain enough information to retrieve the SD in detail.

Sensible constraints are therefore placed on the cloud retrieval problem. Knowing (or trying to retrieve) explicitly the full form of the SD is replaced by targeting cloud water path and effective particle size. Water path has a strong influence on cloud optical thickness, while particle size and shape govern the angular distribution of scattered and emitted radiation. Temperature is also critical for specifying the rate at which a cloud emits/absorbs, scatters, and transmits radiative energy. Some of this energy is shared locally by the cloud with the atmosphere (e.g., atmospheric heating

rates), and some is processed by the Earth's surface (mass and energy exchange processes). In any event we have established a need for retrieving the three most fundamental, wavelength-independent cloud properties: temperature, water path (liquid and/or ice), and effective particle size and shape.

1 Introductory Remarks

Our efforts under this project have three main goals: (1) to develop and refine space-based retrieval methods for cloud top, base, and water path (WP); (2) to infer cloud-water content (WC), effective ice-particle size (D_{EFF}), and visible extinction optical thickness (OT) profiles using visible and thermal infrared data routinely available from all available multinational meteorological satellites; and (3) to compare some retrievals with coincident ground-based lidar and radar observations taken over Hanscom AFB.

Our approach has three main steps: (1) identify cloud phase (water or ice) in imager data using multispectral cloud-detection tests (d'Entremont and Gustafson, 2003); (2) estimate cloud base, top, and liquid/ice-water path (LWP/IWP); and (3) from these estimates infer the liquid/ice-water content (LWC/IWC) and particle-size profiles, which in turn are used to diagnose extinction coefficient profiles for downwelling flux calculations. We begin our discussion with ice-phase clouds and their irregularly shaped particles. Because of their spherical shape, water droplet clouds are substantially easier to model using Mie theory; aside from this, the retrieval approach for water droplets and irregular ice particles exploit similar dependences of multispectral radiances on the cloud-particle microphysics.

1.1 Ice-particle Clouds

Traditional satellite-based retrievals of cirrus IWP are still in the developing stages inasmuch as they can have large uncertainties depending on the type of cirrus size-distribution and ice-particle shapes that are assumed. By way of introduction a deterministic analysis of our retrieval method is summarized here that may have relatively low uncertainties under certain viewing conditions, using several thermal-radiance channels. Those conditions are described along with a mathematically based estimate of expected IWP retrieval accuracies.

Recent research indicates that ice-cloud infrared radiative properties are not always uniquely specified by effective diameter (D_{EFF}) and ice water content (IWC). The size distribution shape, or dispersion, and the degree of bimodality also play an important role at thermal wavelengths (Mitchell, 2002). On the other hand, based on new information on ice particle mass- and area-dimensional relationships, ice particle shape uncertainties now appear to have minimal adverse influence on our cirrus IWP

retrievals (Andy Heymsfield, personal communication). This is because new data show that the geometric cross-section of the ice-particle distributions is similar for bullet rosettes and planar polycrystals, two ice-particle types most commonly observed in cirrus clouds (Korolev et al., 2000). However, this does not preclude having to account for all possible sizes, especially small sizes, in the distribution of cirrus ice particles.

Consequently, our retrieval scheme accounts for a bimodal size-distribution (SD) shape in mid-latitude and tropical cirrus (see Mitchell et al., 2000; Ivanova et al., 2000; Ivanova et al., 2004). We use a bimodal shape for what are termed the small (particles with long-axis diameter D < 100 μm) and large modes (D > 100 μm) of the SD. Here the term "effective diameter" D_{EFF} is meant as the ratio of the third to second moments of the SD. Using a channel centered near 6.7 μm (the water-vapor (WV) band), absorption is a cross-sectional-area dominated radiative process, dependent on the SD and ice-particle shape. At the 12-μm thermal infrared (TIR) the same is true, although generally absorption is stronger here than in the water-vapor band (the imaginary refractive index is higher). In mid-latitudes, model simulations that bracket the natural range of SD variations suggest that a WV-TIR IWP retrieval scheme is accurate to ±15% over an IWP range of 0 to 80 g m^{-2}, and to about ±25% over an IWP range of 80 to 100 g m^{-2} for the coldest cirrus clouds. These accuracies correspond to retrieved 6.7-μm emissivities of ~0.95, along with errors in cirrus temperature that span the natural range of expected values. This is illustrated by the plot on the left side of Figure 1. The plot on the right is for tropical cirrus. In the tropics, WV-TIR IWP retrievals are reliable only out to 50 g m^{-2} or so for very cold cirrus (because the presence of many small particles, with sizes on the order of 10 μm or less, dominate the absorption process), corresponding to cirrus visible extinction optical thicknesses between 3 and 10 (depending more precisely on particle shape and size). The IWP retrieval range extends well beyond 100 g m^{-2} for warmer cirrus, where visible optical thicknesses reach 10 and higher.

Because the 3.9-μm mid-wave infrared (MWIR) imaginary refractive index for ice is quite small (MWIR ~ 0.005, WV ~ 0.05, TIR ~ 0.3), ice-particle cross-sections play a smaller role in governing electromagnetic energy exchange. In the MWIR, absorption is largely an ice-volume-dependent radiative process. This is a handy property to exploit since it reduces IWP retrieval uncertainties due to particle shape, which more strongly govern area-dependent absorption. Radiation-transfer model simulations in mid-latitudes that vary particle size, IWC and cloud depth suggest our IWP retrieval scheme is accurate to about ±15% over an IWP range of 1 to 100 g m^{-2}, and about ±25% over an IWP range of 100 to 200 g m^{-2}, except for very thin cirrus having unusually large crystals or multiple cloud layers. In the tropics the corresponding accuracy ranges are reduced to 110 and 150 g m^{-2}, respectively, which map to cirrus visible extinction optical thicknesses 5 and higher.

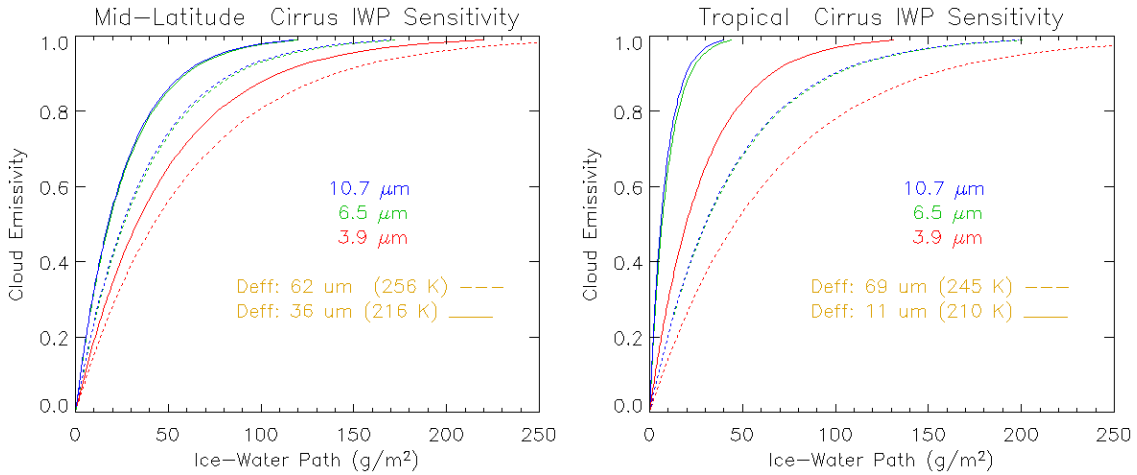

Figure 1. Plots of cirrus IWP as a function of emissivity for mid-latiutude and tropical cirrus size distributions, as prescribed by the SDs of Ivanova et al. (2000)

There are two clear choices for cirrus infrared-based retrievals: WV-TIR and MWIR-TIR. Each has one major advantage and one disadvantage for our particular application. The range of the MWIR-TIR IWP retrieval space is 0-150 g m^{-2}, indicating that MWIR bands offer good sensitivity to cirrus ice-mass estimates, important for accurate heating rate, extinction and radiative-flux calculations. However, in the daytime, MWIR radiances contain both an emitted thermal and a reflected solar component. Since our technique exploits emitted infrared energy, the reflected solar component must be removed from the MWIR cirrus observations before attempting to retrieve cirrus properties with an MWIR-TIR pair. This requires a priori knowledge of attributes such as particle size, optical thickness, and even particle shape since 3.9-μm cirrus reflectances depend on these properties. If these were known properties then there would be no need for real-time cirrus retrievals, obviating the need for MWIR observations. Obviously reflected sunlight is a non-issue at night, so that cirrus retrievals can be performed with MWIR-TIR data whenever the sun is below the horizon. This has the advantage of increasing the sensitivity of our satellite-based techniques to larger IWPs.

Similarly, WV-TIR retrievals have advantages and shortcomings. In mid-latitudes the range of IWP retrieval space is only 0-100 g m^{-2}, but WV radiances are dominated both day and night by cirrus *emission* processes. Thus continuity of cirrus retrievals is maintained across the terminator transition zone since sunlight is not a significant confounder in the WV (and TIR) band. WV-TIR retrievals are the generally preferred channel combination for precisely this reason.

1.2 Water-droplet Clouds

Our water-droplet cloud retrievals are similar to those for ice in that the SD is parameterized by two main attributes: effective particle size and liquid-water path. However water-droplet SDs have a much tighter range of natural variability than do their ice-particle counterparts. They are represented using only a single or mono-modal modified gamma distribution with the same functional form as that for the individual cirrus SD modes. This will be discussed in more detail in Section 6 (in the meantime, see Eq. (5)). In contrast to cirrus particles, the radiative properties of spherical water-droplets have only a weak dependence on the SD dispersion (shape) over their range of naturally observed variability. This is particularly advantageous for reducing uncertainty levels in the overall water-droplet retrievals.

2 Channel Availability and Algorithm Processing Flow in the CDFS Environment

Before proceeding with the algorithm theoretical basis descriptions, it is sensible at this point to summarize the varying combinations of satellite radiance measurements that are routinely available in the CDFS real-time processing environment. Typical global satellite databases include observations from polar and geostationary platforms, both national and international. The composite list in Table 1 comprises the superset of channels available for the purpose of cloud retrievals, and their respective abbreviations will be used repeatedly throughout the text. Also tabulated is the primary cloud-attribute information that each channel provides to the overall retrievals of radiative and microphysical products.

In Table 2 are listed the common channel combinations available on all CDFS satellite platforms as a function of time of day. These combinations dictate algorithm processing flow: for several reasons, the use of infrared data both day and night is favored over combined visible/infrared techniques by day and infrared by night. First, using infrared channels universally that are not "contaminated" by solar energy means that the cloud analyses will have smooth, undetectable boundaries across the terminator. A day-night retrieval bias is also likely diminished. Whenever visible data must be used to infer optical thickness and/or liquid/ice-water path, an abrupt change tends to exist across the terminator in the spatial coherence of the various cloud microphysical properties (and to some degree, the cloud and cloud-phase mask itself, as identified in previous sections). Third, for all CDFS platforms, the solar channels are not absolutely calibrated on board. Most channels are vicariously calibrated (which helps), but their absolute accuracies remain suspect and, by association, so do the

corresponding retrievals. Add to this the issue of cloud mutual and self shadowing and

Approximate Wavelength	Band Name	Dominant Source	Value to Cloud Retrievals	Platforms
0.63 μm	VIS	Visible Solar	Optical Thickness	All
0.86 μm	NIR	Near-infrared Solar	Optical Thickness	TIROS, MSG
1.61 μm	SWIR	Shortwave-infrared Solar	Particle Effective Size	TIROS, MSG
3.8 μm	MWIR	Midwave-infrared: Solar/Thermal Cusp	Liquid/Ice-water Path	TIROS, MSG, GOES, MTSAT
6.7 μm	WV	Water Vapor Thermal	Optical thickness, Effective temperature	GOES, MSG, MTSAT
8.55 μm	LWIR	Longwave infrared Thermal	Particle Effective Size, Shape	MSG
10.8 μm	TIR	Thermal infrared	Optical thickness, Effective temperature	All
12.0 μm	TIR	Thermal infrared	Optical thickness, Effective temperature	All
13-15 μm	CO2	Carbon Dioxide Thermal	Particle Effective Size, Shape	GOES, MTSAT

Table 1. List of the sensor bands used in our algorithms for the retrieval of cloud spatial, radiative, and microphysical properties

it is easy to see that the use of visible data in direct relation with one-dimensional radiative-transfer theory is somewhat problematic.

Satellite	Daytime band combination	Nighttime band combination
GOES	VIS, MWIR, WV, TIR, CO2	MWIR, WV, TIR, CO2
MSG	VIS, NIR, SWIR, WV, LWIR, TIR (2), CO2	WV, LWIR, TIR (2), CO2
METEOSAT	VIS or WV, TIR	WV, TIR
MTSAT	VIS, MWIR, WV, TIR (2)	MWIR, WV, TIR (2)
TIROS – 18	VIS, NIR, SWIR, TIR (2)	MWIR, TIR (2)
TIROS (all others)	VIS, NIR, MWIR, TIR (2)	MWIR, TIR (2)
DMSP	VIS, broadband TIR	Broadband TIR

Table 2. Channel-set combinations for each of the CDFS satellites, as a function of time of day

Algorithm flow decisions are based on channel set availability. When inspecting Table 2 keep in mind that under all tabulated conditions the cloud retrievables are: cloud-particle effective diameter D_{EFF} (defined as the ratio of the third and second moments of the SD), cloud liquid/ice-water path, and cloud physical temperature. All other attributes such as cloud top/base and emissivity are either diagnosed or inferred from these basic three using the theories outlined in coming sections. Other important flux-driving radiative properties such as single-scattering albedo ω_o and asymmetry parameter g are tied to SD and particle-shape constraints that must be made at the outset of the retrieval process, due to the availability (or lack thereof) of information contained in the available set of upwelling radiances. Details of these constraints are left for future sections wherein their impact on the retrieval process is more formally presented and their overall context better understood.

In the CDFS environment, processing flow can take several paths as summarized in Table 3. The most constrained (most "simple") retrieval path is invoked when only a single channel of infrared data are available, as presented in Section 4. Another path exploits pairs of infrared bands that have no contribution from the sun – i.e., nighttime MWIR and TIR, or day/night WV, LWIR, and/or TIR. These are infrared-only retrievals whose deterministic attributes are described in Section 5. Still other flow paths are used when only one thermal infrared band is available during the daytime in combination with one or several reflected-solar bands. These paths are described in Section 6.

Before continuing we establish some notational conventions that will be used throughout the remainder of this paper.

Satellite	Daytime algorithm path	Description	Nighttime algorithm path	Description
GOES	WV – TIR	Section 5	WV – TIR	Section 5
MSG	WV – TIR	Section 5	WV – TIR	Section 5
METEOSAT	VIS – TIR WV – TIR	Section 6a Section 5	WV – TIR	Section 5
MTSAT	WV – TIR	Section 5	WV – TIR	Section 5
TIROS – 18	NIR/SWIR - TIR	Section 6a	MWIR - TIR	Section 5
TIROS (all others)	NIR - TIR	Section 6b	MWIR – TIR	Section 5
DMSP	VIS – TIR	Section 6b	TIR	Section 4

Table 3. List of cloud-retrieval processing flow by satellite platform, as prescribed by sensor-data availability

3 Notation

$B_\lambda(T)$ Planck blackbody monochromatic radiance, W m^{-2} μm^{-1} $ster^{-1}$
$B_N(T)$ Planck blackbody equivalent monochromatic radiance for satellite sensor band "N," W m^{-2} μm^{-1} $ster^{-1}$
D_{EFF} Ice-particle effective diameter, μm
ε Effective emissivity, dimensionless
I_N Band-weighted upwelling infrared radiance, W m^{-2} μm^{-1} $ster^{-1}$
λ Wavelength, μm
M, N Sensor channel designations
Q_{ABS} Absorption efficiency factor, dimensionless ratio of radiative and physical cross sections
$R_N(\lambda)$ Response function for band "N," dimensionless
T Temperature, K
τ Optical thickness, dimensionless
t Transmittance, dimensionless
z Height, m

4 Single-channel TIR Retrievals

The most constrained cloud retrievals occur under conditions wherein only TIR channel data are available for processing. Although this is possible with any satellite, in practice the only time it happens is with DMSP during the night half of an orbit. In this case many constraints must be forced upon the retrieval in order to make up for the lack of cloud information contained in the single-channel thermal radiance observations. The first is that the cloud, be it in the liquid or ice phase, is assumed to be nearly a blackbody. Since its emissivity is very close to one, its brightness temperature is an almost precise measure of the true physical temperature T_{CLD} of the cloud. This temperature is converted to cloud top by means of comparison with a collocated NWP temperature profile.

In the case of water clouds an effective size is assumed (currently set at D_{EFF} = 17 μm, a sort of globally representative average value) along with a high value of 0.55-μm extinction optical thickness (currently set to $\tau_{EXT,VIS}$ = 12), in keeping with the assumed blackbody nature of the cloud. For cirrus clouds to $\tau_{EXT,VIS}$ is also set to 12, but we have exploited a means of estimating D_{EFF} in tropical anvil and mid-latitude cirrus as a function of cirrus environmental temperature T_{CI} (Mitchell et al., 2000; Ivanova et al., 2000, 2004 – this too will be discussed in more detail later). Thus there is a one-to-one mapping between D_{EFF} and T_{CI}.

The remaining unknown – cloud liquid/ice-water path (LWP or IWP) – can be inferred from the visible extinction optical thickness $\tau_{EXT,VIS}$ using the geometric optics relation $\tau_{EXT,VIS}$ = 3 LWP / (ρ_{WAT} D_{EFF}) – or, for ice clouds, $\tau_{EXT,VIS}$ = 3 IWP / (ρ_{ICE} D_{EFF}) – where ρ is the density of ice or water, as dictated by cloud phase.

5 Cirrus Infrared Radiative Transfer Model

The observed upwelling infrared radiance $I_{OBS,N}$ in satellite channel "N" for an infinitesimally thin, non-reflecting cirrus slab is expressed in terms of the cirrus bulk emissivity ε_{CI} as

$$(1) \qquad I_{OBS,N} = (1 - \varepsilon_{CI,N}) I_{CLR,N} + \varepsilon_{CI,N} B_N (T_{CI}) t_{ATM,N} ,$$

where "t_{ATM}" is the atmospheric transmittance between cirrus top and TOA, typically prescribed using radiative transfer codes and NWP water-vapor and temperature soundings. Conditions under which (1) is valid are discussed in later sections. For now, we shall assume that cirrus radiance observations from two window channels are available.

5.1 Formulating the Retrieval Problem

The quantities ε_{CI} and T_{CI} in Eq. (1) are descriptors of the spatial, radiative, and microphysical properties of a cirrus cloud. Exploiting a cloud mask (see d'Entremont and Gustafson, 2003) to identify nearby cirrus-free radiances provides an estimate for $I_{CLR,N}$, leaving two unknowns in emissivity and effective temperature. With only one equation the solution is mathematically ill-posed; it is necessary to add at least one more equation (constraint) to the problem. Consider writing (1) for two wavelength window bands "N" and "M," yielding

$$(2a) \qquad I_{OBS,N} = (1 - \varepsilon_{CI,N}) I_{CLR,N} + \varepsilon_{CI,N} B_N (T_{CI}) t_{ATM,N}$$

and

$$(2b) \qquad I_{OBS,M} = (1 - \varepsilon_{CI,M}) I_{CLR,M} + \varepsilon_{CI,M} B_M (T_{CI}) t_{ATM,M} \ .$$

At the outset this appears to be a well-posed set of two equations in two unknowns ε_{CI} and T_{CI}. However the cirrus emissivity $\varepsilon_{CI,X}$ is a wavelength-variant quantity with dependences on the imaginary refractive index at wavelength λ_X, as well as on ice-particle size and shape, and the nature of the bimodal size distribution N(D). Thus in introducing a second equation we have also introduced a new unknown in $\varepsilon_{CI,M}$. It is therefore necessary to relate $\varepsilon_{CI,M}$ to the other "original" unknowns $\varepsilon_{CI,N}$ and/or T_{CI}. This need motivates the development of an absorption theory for non-spherical ice crystals that is outlined next.

5.2 Modeling Cirrus Microphysics

A deterministic relationship is described here among effective particle size, cirrus temperature, and the cirrus emissivities at multiple wavelengths. Each of these is addressed individually in the following sections, and then combined into one cohesive theory useful for solving the simultaneous set of Eqs. (2a) and (2b).

By way of introduction effective diameter (D_{EFF}) and the anomalous diffraction theory of van de Hulst (1981) turn out to be important concepts in our modeling approach, as they relate our retrieved quantities with other variables of interest such as cirrus ice water content (IWC) and ice-water path (IWP). We begin therefore with the cirrus ice-particle size distribution.

5.2.1 Ice-Particle Effective Diameter

We define effective diameter D_{EFF} with respect to irregularly shaped ice crystals as the ratio of the third and second moments of the size distribution N(D), where D is the long-axis dimension of an ice particle. Conceptually its meaning can be understood

using the concept of effective distance or photon path, d_E. This is the particle volume-to-area ratio as first suggested by Bryant and Latimer (1969), and further developed in Mitchell (200x) to treat absorption and extinction by ice particles. In these studies d_E is defined as the particle volume V at bulk ice density divided by the particle's projected area P at random orientation:

$$d_E = m / (\rho_{ICE} P) , \quad (3)$$

where m is the particle's mass, and bulk ice density $\rho_{ICE} = 0.92$ g cm^{-3}. This value of ρ_{ICE} must be used since the ice refractive indices we employ in our models are referenced to bulk ice density. This concept of d_E is borne out of the anomalous diffraction approximation (ADA), a simplification of Mie theory (van de Hulst, 1981). Absorption processes represented in ADA are based on the principle of effective photon path, indicating that d_E is the relevant dimension for autonomous particle-radiation interactions.

We can take this one step further and relate the diameter of a sphere, D, to its effective distance (expected photon path length), d_E. Using ice spheres as an example in (3), mass $m = \rho_{ICE} (\pi D^3/6)$ and projected area $P = \pi D^2/4$, giving

$$d_E = 2/3 D . \quad (4)$$

If there is an effective photon path for a single particle, it can be asked if there is also an effective photon path D_E for the *collection* of ice particles that comprise the cirrus. A gamma size distribution is the one most often used to describe the number of cirrus ice particles with effective diameter D:

$$N(D) = N_o D^v e^{-\Lambda D} , \quad (5)$$

with dispersion and slope parameters v and Λ, respectively. Based on the formalism used in Eq. (3) but extended to the entire distribution of ice particles,

$$D_E = IWC / (\rho_{ICE} P_{TOT}) , \quad (6)$$

where IWC is the cirrus ice-water content (ice mass per unit volume), and where P_{TOT} is the total projected area of all ice particles in the size distribution (with units of area per unit volume; e.g., cm^2 cm^{-3} = cm^{-1}). In other words, projected area P_{TOT} is the geometric cross-sectional area per unit volume of a distribution (5) of non-overlapping ice particles with random orientations. Based on Eq. (4), the effective diameter of the size distribution should then be 3/2 d_E or

(7) $$D_{EFF} = 3\ IWC / (2\ \rho_{ICE}\ P_{TOT}) .$$

Mitchell (2002) continues on from this point to show that there is one general definition for effective diameter, $\int D^3\ N(D)\ dD / \int D^2\ N(D)\ dD$, for all clouds regardless of phase, and that this definition can be understood physically as the representative photon path for the collection of particles in the size distribution. In the next section the relationship between cirrus absorption efficiency and effective diameter is described.

5.2.2 Absorption of Infrared Radiation by Ice Clouds

ADA approximates the absorption efficiency $Q_{ABS,ADA}$ for a single ice particle as

$$Q_{ABS,ADA} = 1 - \exp(- 4\pi\ n_I\ d_E / \lambda) ,$$

where n_I is the imaginary part of the refractive index at wavelength λ. As defined in Eq. (4), d_E is the representative distance a photon travels through a particle without the occurrence of internal reflections or refraction. Substituting Eq. (4) for $d_E = 2/3\ D_{EFF}$ into the above expression yields

(8) $$Q_{ABS,ADA} = 1 - \exp(- 8\ \pi\ n_I\ D_{EFF} / 3\lambda) ,$$

where $Q_{ABS,ADA}$ is now the geometric-optics absorption efficiency representing the entire size distribution based on ADA and the concept of effective photon path.

This expression describes mathematically the absorption due only to a size distribution's geometric cross section. Mitchell (200y) shows that relevant particle-radiation interaction processes not accounted for by ADA can be parameterized in terms of ADA such that this modified ADA yields absorption efficiencies with errors ~10% or less relative to Mie and T-matrix theory. Namely, Eq. (8) has been expanded by Mitchell (200y) to include the processes of internal reflection/refraction and photon "tunneling," which collectively is well approximated by

(9) $$Q_{ABS} = (1 + C_1 + C_2)\ Q_{ABS,ADA} .$$

The leading term (the "1") on the right side of Eq. (9) represents absorption solely by virtue of the particle's geometric cross section; the term C_1 accounts for absorption due to internal reflection and refraction; and C_2 is the "photon tunneling" term. Tunneling is a process by which photons from beyond the particle's geometric cross-section are funneled (via wave-wave interactions) in toward the ice particle where they may be absorbed, internally reflected, refracted, or transmitted. For spheres, Mie theory

prescribes the "tunneling factor" as 1; for irregularly shaped ice particles, this factor lies between 0 and 1, depending on particle shape. The term "C_2" above contains dependences on this tunneling factor. It turns out for any given particle shape that tunneling is strongest at wavelengths where real refractive indices are highest. See Appendix A for a more detailed discussion of tunneling.

Expressions for the constants C_1 and C_2 are given in Mitchell (200y) and are not repeated here, except to note that they depend on ice-crystal particle size, shape, wavelength, and index of refraction.

The coefficient for absorption by a randomly oriented ice particle is defined as

$$\beta_{ABS} = \int_0^\infty Q_{ABS}(D,\lambda)\, P(D)\, N(D)\, dD \,, \tag{10}$$

where Q_{ABS} is the absorption efficiency at wavelength λ for ice crystals of effective diameter D, P(D) is the projected area for a crystal of dimension D, and N(D) is the ice-crystal particle size distribution as given by Eq. (5). If D_{EFF} is the appropriate dimension for describing particle-radiation interactions for an entire size distribution, then it is natural to ask what the consequences might be if the absorption efficiency Q_{ABS} were to be taken outside the integral of (10) and expressed in terms of D_{EFF} such that the absorption coefficient is precisely prescribed. This results in the following simple equation

$$\beta_{ABS} = \overline{Q}_{ABS}\, P_{TOT} \,, \tag{11}$$

where $\overline{Q}_{ABS}$ is the absorption efficiency representing the entire size distribution; and where

$$P_{TOT} = \int_0^\infty P(D)\, N(D)\, dD \tag{12}$$

is the geometric cross-section area of the entirety of randomly oriented ice particles in the cirrus cloud, with units of area per unit volume (e.g., $cm^2\ cm^{-3} = cm^{-1}$). For irregularly shaped crystals it is easy to comprehend that P(D) is a function of crystal shape and size. Using the projected-area dimensional power law expression $P = \sigma D^{\delta}$ (see Mitchell, 1996; 200z) for class of ice crystals of a given shape, and substituting Eq. (5) for N(D) into Eq. (12) yields

(13) $$P_{TOT} = \int_0^\infty \sigma N_o D^{\delta+v} e^{-\Lambda D} dD .$$

This in turn can be integrated analytically to yield

(14) $$P_{TOT} = \sigma N_o \Gamma(\delta+v+1) / \Lambda^{\delta+v+1} .$$

Solving Eq. (11) for absorption efficiency finally yields

(15) $$\overline{Q}_{ABS} = \beta_{ABS} / P_{TOT} .$$

The absorption coefficient β_{ABS} and the cross-sectional area P_{TOT} of the entire size distribution are dependent on both the amount and shape of the ice particles that comprise the cirrus cloud. However, the absorption efficiency $\overline{Q}_{ABS}$ is a normalized metric of absorption that depends only on crystal size, shape, wavelength, and refractive index.

Mitchell (200x) has derived an analytic expression for β_{ABS} for a "representative" unit volume of actual ice-crystal size distributions, with explicit dependences

(16) $$\beta_{ABS} = \beta_{ABS} (\sigma, \delta, v, \Lambda)$$

on the area power-law ($P = \sigma D^{\delta}$) and size-distribution parameters σ, δ, v, and Λ. A detailed analysis of Eq. (16) is not repeated here (see Mitchell, 200x) except to note with importance that the absorption coefficient β_{ABS} is dependent on the shape of the size distribution N(D) as prescribed by the dispersion and slope parameters v and Λ, respectively; and on ice-crystal shape as well via the projected-area power-law coefficients σ and δ. Recall now the introductory remarks concerning cross-sectional area and ice-particle shape. Their explicit mathematical form is not detailed here; nonetheless the dependences noted in Eq. (16) offer physical and mathematical insight into the importance of the wavelength-independent properties of ice-particle size and shape, as well as the modified gamma distribution parameters.

With a means available for computing β_{ABS} and P_{TOT}, their ratio yields a distribution's absorption efficiency $\overline{Q}_{ABS}$ for the entire SD as prescribed by Eq. (15). Such computations have been performed and compared with numerical Mie theory integrations over size distributions of water droplets, and against observations of

absorption efficiencies for non-spherical ice crystals (see Mitchell, 200w); Figure A1 in Appendix A shows the comparison results. Errors relative to $\overline{Q}_{ABS,MIE}$ are low (generally within 10%); and for small ice crystals grown in a cloud chamber the errors between observation, T-matrix calculations, and the modified ADA theory are within 3% at wavelengths between 2 and 18 μm (Mitchell, 200w). With an approach in hand for computing absorption efficiency, a basis is established for computing cirrus infrared emissivities in our retrieval paradigm, which is outlined next.

5.2.3 Cirrus Emissivity

One of the major elements of our retrieval set [as defined by simultaneous solution of Eqs. (2a) and (2b)] is the estimated emissivity ε at the thermal infrared reference wavelength 11 μm. Assuming no scattering at the WV and TIR wavelengths,

$$\varepsilon = 1 - \exp(-\tau_{ABS} / \cos \theta_{SAT}) , \quad (17)$$

where θ_{SAT} is the satellite zenith angle and τ_{ABS} is the absorption optical depth. Dividing optical depth by the factor $\cos \theta_{SAT}$ adjusts the path length through the cirrus for non-nadir views. For an infinitesimally thin cirrus cloud where the size distribution is invariant with in-cloud position, the absorption optical depth is given by

$$\tau_{ABS} = \beta_{ABS} \Delta z , \quad (18)$$

where Δz is the cloud physical depth (from base to top) and β_{ABS} is the absorption coefficient, represented here by Eq. (16) and fully defined in Mitchell (200x). The assumption of an invariant size distribution is consistent with our idealized cirrus thin-slab assumption (recall Eq. (1)), but it can introduce potential errors that are discussed further along in the applications sections.

5.2.4 Ice Water Path

Equation (7) can now be exploited to solve for the ice water path IWP, which is the melted-equivalent water mass per unit area of a vertical column through the entire extent of the cirrus cloud. By definition, and assuming that IWC is the vertically averaged value,

$$IWP = IWC \ \Delta z$$

and Eq. (7) becomes

$$D_{EFF} = 3 \ IWP / (2 \ \rho_{ICE} \ P_{TOT} \ \Delta z) . \quad (19)$$

Solving for β_{ABS} in Eqs. (11) and (18) and equating the two expressions gives

$$P_{TOT} = \tau_{ABS} / (\overline{Q}_{ABS} \Delta z) .$$

Inserting this result into (19) for P_{TOT} and solving for ice-water path,

(20) $$IWP = 2 \rho_{ICE} D_{EFF} \tau_{ABS} / (3 \overline{Q}_{ABS}) .$$

Substituting (20) for τ_{ABS} in (17), the cirrus emissivity is expressed as

(21) $$\varepsilon = 1 - \exp[-3 IWP \overline{Q}_{ABS} / (2 \rho_{ICE} D_{EFF} \cos \theta_{SAT})].$$

Solving Eq. (21) for IWP yields

(22) $$IWP = - 2 \rho_{ICE} D_{EFF} \cos \theta_{SAT} \ln(1 - \varepsilon) / (3 \overline{Q}_{ABS}) .$$

Note that D_{EFF} dependencies are indicated both in the numerator and in the denominator of Eq. (22), since $\overline{Q}_{ABS}$ is dependent on particle size effective diameter via Eq. (8).

5.2.5 Visible Extinction Optical Thickness

The extinction coefficient (absorption plus scattering) is defined mathematically as

$$\beta_{EXT} = \int_0^\infty Q_{EXT}(D,\lambda) P(D) N(D) dD .$$

At visible solar wavelengths ($\lambda \approx 0.5$ μm) it is well known that the extinction efficiency $Q_{EXT,VIS}$ is accurately approximated as 2 for ice particles in cirrus (and for spherical water droplets, too). This corresponds to size parameters $\pi D / \lambda \geq 30$. At and near wavelengths of 0.5 μm, size parameters greater than 30 correspond to size-distribution effective diameters $D_{EFF} > 5$ μm. Ice particles as observed in natural cirrus always satisfy this condition, even at the tropical tropopause; and cloud water droplets are always larger than this. With $Q_{EXT,VIS} = 2$ and using the definition for P_{TOT} in (12), the above expression for the visible extinction coefficient can be written

$$\beta_{EXT,VIS} = 2 P_{TOT} .$$

Solving Eq. (7) for P_{TOT} and noting that the extinction optical thickness $\tau_{EXT,VIS} = \beta_{EXT,VIS} \Delta z$, we have finally that

(23) $$\tau_{EXT,VIS} = 3 IWP / (\rho_{ICE} D_{EFF}) .$$

5.2.6 Numerical Considerations

With an expression now in hand to compute emissivity at any wavelength, as prescribed by (21), let's re-examine the original problem of two equations in three unknowns $\varepsilon_{CI,M}$, $\varepsilon_{CI,N}$, and T_{CI}. In Eq. (21) it is seen that several new unknowns have been introduced to the set of equations, including D_{EFF}, IWP, and the coefficients σ, δ, ν, and Λ. Instead of helping to bring the number of equations and unknowns into line, it seems that there are now even more unknowns (the aforementioned six plus T_{CI}) than equations [three: (2a), (2b), and (21)].

Fortunately, we have exploited a means of estimating the size-distribution dispersion and slope parameters ν and Λ, and consequently D_{EFF}, in tropical anvil and mid-latitude cirrus as a function of cirrus environmental temperature (Mitchell et al., 2000; Ivanova et al., 2000, 2004). The tropical scheme is based on 93 size distributions from three tropical anvils reported in McFarquhar and Heymsfield (1997) for the CEPEX field campaign, three tropical anvils reported in Knollenburg et al. (1993), and a tropical tropopause cirrus case (Heymsfield, 1984). The mid-latitude scheme is based on over 1000 in-situ measurements of cirrus taken during ARM and FIRE campaigns in the central U.S. (Ivanova et al., 2000). Exploiting this parameterization means that D_{EFF} and the SD dispersion and slope coefficients ν and Λ are all explicit functions of temperature T_{CI} only. Notationally,

(24a) $$D_{EFF} = D_{EFF}(T_{CI}) ,$$

(24b) $$\nu = \nu(T_{CI}) ,$$

and

(24c) $$\Lambda = \Lambda(T_{CI})$$

as prescribed by Ivanova et al. (2000) and illustrated in Figure 2. The projected-area power-law coefficients σ and δ are functions of an assumed particle shape as tabulated by Mitchell (2002) [we usually pick planar polycrystals or bullet rosettes, cited as most

common in nature by the recent literature (Korolev, 2000)]. If at some future time it is found that ice-particle shape is strongly dependent on cirrus environmental temperature, this easily can be incorporated into our retrieval algorithm. Fortunately, in the meantime, the difference in geometric and radiative properties between polycrystals and rosettes is small (Andy Heymsfield, personal communication).

Exploiting these temperature-size-shape relationships reduces the number of equations/unknowns to 3/4, seemingly leaving only ice water path as the "extra" variable. However the numerical approach to solving the three simultaneous equations is fundamentally one of repeatedly guessing at the set { $\varepsilon_{CI,N}$, $\varepsilon_{CI,M}$, T_{CI} } until it satisfies simultaneously the full set of equations. Thus all we need is a way to obtain $\varepsilon_{CI,M}$ *given* a guess value $\varepsilon_{CI,N}$. Writing Eq.(24) for two wavelengths λ_N and λ_M and setting the wavelength-invariant "IWP = IWP" results in

$$-2\,\rho_{ICE}\,D_{EFF}\cos\theta_{SAT}\ln(1-\varepsilon_{CI,N}) / (3\,\overline{Q}_{ABS,N}) = -2\,\rho_{ICE}\,D_{EFF}\cos\theta_{SAT}\ln(1-\varepsilon_{CI,M}) / (3\,\overline{Q}_{ABS,M}) .$$

All the wavelength-independent quantities cancel during simplification leaving

$$\varepsilon_{CI,M} = 1-(1-\varepsilon_{CI,N})^{R} , \tag{25a}$$

where the absorption-efficiency-ratio exponent R is defined as

$$R = \overline{Q}_{ABS,M} / \overline{Q}_{ABS,N} . \tag{25b}$$

Since the absorption efficiencies $\overline{Q}_{ABS}$ are dependent on effective particle size [see Eq. (19)], the N(D) dispersion, and its slope [recall Eqs. (14) and (16)], and since each of these is a function only of the cirrus temperature [via Eq. (24)], then $\overline{Q}_{abs}$ is expressible as a function of T_{CI} as well, along with the ratio R:

$$\overline{Q}_{ABS}(D_{EFF},\lambda) \equiv \overline{Q}_{ABS}[\,D_{EFF}(T_{CI}),\lambda\,] \equiv \overline{Q}_{ABS}(T_{CI},\lambda) . \tag{26}$$

We have finally reduced the mathematical problem to one of three equations [(13a), (13b), and (25)] in three unknowns $\varepsilon_{CI,N}$, $\varepsilon_{CI,M}$, and T_{CI}. Cirrus IWP is thus a diagnostic, derived product of the retrieval; i.e., once the emissivity is found it can be used with Eq. (22) to retrieve ice water path (or vice versa via Eq. (21)).

The numerical recipe of our cirrus retrieval algorithm is reviewed here. Given

imager radiance data with two thermal infrared window bands centered on wavelengths λ_N and λ_M, along with a pre-computed pixel-level cloud mask that identifies all cirrus clouds, then:

(a) Use the cloud mask (e.g., d'Entremont and Gustafson, 2003) to compute nearby averages of the cirrus-free radiances $I_{CLR,N}$ and $I_{CLR,M}$ for each cirrus pixel, based on the background geography type;

(b) Guess at the set { IWP, T_{CI} } of cirrus ice-water path and temperature. Use T_{CI} to determine D_{EFF}, v, Λ, Q_{ABS} (D_{EFF} , λ_N) = $\overline{Q}_{ABS,N}$, and $\overline{Q}_{ABS,M}$ as described in this section, and compute $\varepsilon_{CI,N}$ as prescribed by Eq. (21);

(c) Using (25), compute the ratio R and the value of $\varepsilon_{CI,M}$ that is physically consistent with with $\varepsilon_{CI,N}$; and

(d) Check to see whether the guess set { IWP, T_{CI} } of cirrus attributes satisfies Eqs. (2a) and (2b) simultaneously for the satellite radiance observations $I_{OBS,N}$ and $I_{OBS,M}$ in bands "N" and "M" for the cirrus pixel in question. If so, stop. If not, re-iterate starting at Step (b).

The question of how to iterate on a guess is an important one if computational timeliness is an issue. Binary search techniques or "brute-force" methods that consider all mathematically plausible combinations of { IWP, T_{CI} } are two possible strategies. We use a hybrid of these two options and retrieve cirrus properties at speeds of 10^{-5} sec per pixel on a PC with a Linux OS.

Figure 3 illustrates graphically the process of retrieving cirrus ice-water path and effective temperature. Plotted for the WV and TIR infrared bands are all mathematically possible pairs of IWP and T_{CI} for a given set of satellite radiance observations. The radiance observations correspond to a 6.5-μm WV brightness temperature of 227.8 K, and a 10.7-μm TIR temperature of 247.5 K. Note that for a single sensor band the number of theoretically possible pairs { IWP, T_{CI} } is infinite. This ambiguity is resolved, however, by choosing the pair that satisfies the satellite upwelling radiance equations simultaneously at the two infrared wavelengths. This is the fundamental basis of our infrared retrieval paradigm.

6 Estimates of Cloud Top and Base

With a method now in place for determining cloud effective temperature and, by way of NWP RAOBs, the cloud effective height, the next step is to estimate cloud top

and base. Our retrievals of cloud top and cloud base are based on pixel-level retrievals of the emissivity-adjusted effective cloud temperature T_{CI} in Eq. (2). Eventually this temperature is converted to altitude using satellite-coincident NWP upper-air forecasts of temperature, pressure, and geopotential.

Once the pixel-level effective temperatures are computed, we exploit the "local" texture of the effective-temperature retrievals to estimate cloud top and cloud base. For cloud vertical boundaries we look at the effective temperatures of pixels "near" the edges of a cloud mass. By "near" is meant "those pixels that lie within a prescribed, tunable radius of the analysis pixel." Currently this radius is set in our production runs (see www.aer.com/cloud) by default to ten 5-km GOES infrared pixels for both cloud base and cloud top. A frequency distribution of these temperatures is assembled for all pixels within the tunable radius, and the base-temperature (top-temperature) estimates

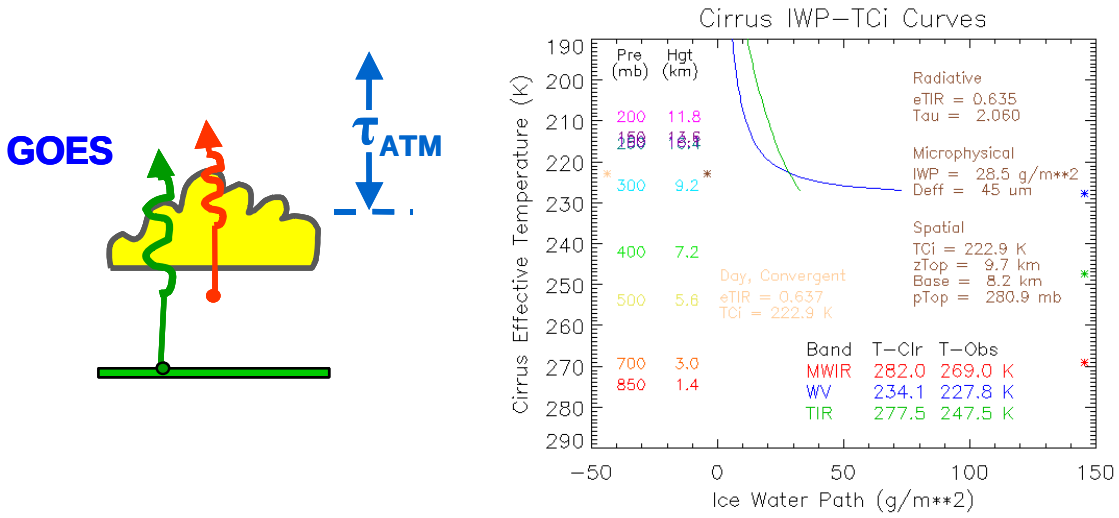

Figure 3. Graphical depiction of the retrieval method outlined in Section 5.2.6. The curve crossing point denotes the cirrus IWP and temperature retrieval for this pixel.

are assigned as the mean of the temperatures that fall above (below) the median effective temperature of the local histogram.

Horizontal irregularities in satellite-derived effective temperature retrievals are based on lots of small-magnitude influences: sensor noise, an incorrect estimate of the cloud-free radiance (I_{CLR} in Eq. (2)), and inaccurate NWP T-z soundings name a few. Nonetheless we exploit the spatial structure of the "raw" pixel-level effective temperature retrievals to infer cloud top (usually within a very localized region) and cloud base (within a more "regional" region), for both water-droplet and ice-particle clouds. At the moment we use no information from the NWP upper-air profiles other

than to convert the base and top temperatures to height. Although empirically based, we observe some diagnostic skill in this texture-based approach, as is illustrated next.

7.1 GOES Cirrus Retrievals and Ground-Based Lidar/Radar Observations

As mentioned in the introductory sections, satellite and ground-based cirrus observations for more than two dozen case days were collected over Hanscom AFB near Boston, MA during 2005, including vertically pointing ground based radar and lidar along with radiosondes and environmental satellites. The data collection periods have been event driven, based on the presence of at least one cirrus cloud layer visible to the eye over the Hanscom site. Because of the emphasis on cirrus transmittance, the basic go/no-go criteria for any given day was "the presence of at least one broken or overcast cirrus layer, in the absence of scattered low and middle clouds." The cloud cover should be of at least three hours duration, to allow at least ½ hour of AFCPR (Air Force Cloud Profiling Radar) 35-GHz radar and PEELS (Portable Eye-Safe Environment Lidar System) 1.574-μm lidar operation before a radiosonde launch and 2½ hours after. Each declared observing day has at least one 3-hour observing period.

A total of 27 days have met measurement criteria and at least three-hours of observations were collected each day. We have used this unique data set to evaluate the performance of our cirrus extinction and IWC-profile retrieval algorithm using coincident GOES-12 cirrus analyses. During the measurement periods, GOES-12 (GOES East) satellite data are analyzed using the technique outlined in Sections 3 and 4.1 to retrieve the set of cirrus bulk properties listed in Table 4, at the GOES infrared pixel level (with a nominal 4-km spatial resolution at satellite subpoint).

- Cloud mask, cloud phase (ice or water)
- Effective temperature/height/pressure
- Cloud top
- Cloud base
- IWP/LWP
- Effective particle size
- Mass-median particle size
- Visible extinction optical thickness
- Infrared emissivity (at 11 μm)

Table 4. List of the cirrus bulk (total-column) properties retrieved by the algorithm outlined in Section 5

Our satellite retrievals have an update frequency of at least 15 minutes – though many of the cases occurred during so-called "super rapid scan" periods where the

update frequency can be as short as a few minutes. Using the GOES data, three-dimensional profiles of extinction and effective ice-particle size are generated as follows.

With an estimate in hand for cirrus top and base, along with a parameterization of effective ice-particle size as a function of the cirrus environmental temperature, the cirrus optical thickness at some level z* in the cloud is given by Eq. (23) as

$$\tau_{EXT,VIS} = 3\, IWC(z^*)\, \Delta z / (\rho_{ICE}\, D_{EFF}) , \quad (27)$$

where IWC(z*) is the cirrus layer ice-water content at level z*, Δz is the layer physical thickness (the "IWP" in Eq. (23) equals "IWC(z*) Δz"), and D_{EFF} is the layer's SD effective particle size. It follows that the extinction coefficient $\beta_{EXT,VIS}$ at level z* within the cirrus is simply

$$\beta_{EXT,VIS}(z^*) = 3\, IWC(z^*) / (\rho_{ICE}\, D_{EFF}) . \quad (28)$$

All that is required to compute Eq. (28) is a satellite-estimated profile of IWC.

Obviously the GOES total-column cirrus radiance observations and IWP retrievals offer little insight as to the nature of the IWC *vertical profile*. However the integrated IWC, or namely the IWP, is a retrievable. To solve the problem of IWC we applied an a-priori knowledge of IWC profile shape using the in-situ radar and lidar observations. We developed a "climatology" of sorts of the radar backscatter and lidar extinction profile shapes using data from the first twenty case-study days. If we assume that the IWC profile shape is the same as the lidar and radar-profile observation average shapes, then the average shape as a function of cirrus physical thickness provides insight into the nature of the IWC profile *shape*. We understand that the correspondence between radar/lidar observation and IWC is not precisely one-to-one. The relation between IWC and attributes like ice-particle size and shape makes the validity of such a direct comparison less tenuous. However, we are pressed with a requirement to generate cirrus extinction coefficient profiles from satellite.

This is the approach we decided to take: with an estimate of cirrus top, base, and an observations-based IWC-profile shape, we assign an absolute IWC(z*) profile (required by Eq. (28)) by constraining the normalized IWC profile to integrate vertically to the retrieved total-column IWP. Figure 3 contains the lidar and radar-based normalized IWC profiles that were observed between cirrus base and top for all observations made during the early portion of the 2005 measurement period, plotted as a function of cirrus physical thickness. Currently we use the 1-to-2.5-km IWC profile shape in our retrievals. Future upgrades will include prescribing IWC shape based on

the GOES-retrieved cirrus base and top estimate (i.e., based on the retrieved cirrus physical thickness).

Figure 4 contains a plot of the retrievals for a seven-hour collection period on 29 July 2005. The figure shows direct comparisons between the lidar return, depicted as the color-coded watermark image in the background, and coincident satellite-based retrievals from our cirrus bulk-property retrieval algorithms (see Table 1). Diamonds (squares) denote our cloud-top (base) retrievals, and the red triangles denote the cirrus effective-temperature (radiative "center-of-mass") estimate for the GOES pixel directly over the lidar. Note that the balloon sounding made near the beginning of the observation period and shown on the right of the figure also shows skill at identifying the height of the cirrus base and top (more later). The tabulated values listed below the lidar image are a time series of pixel-level retrievals for the cirrus cloud that was closest to Hanscom for that particular time. Each row is interpreted as follows: **eTIR** is the 11-μm emissivity times 100 (e.g., 35 means 0.35); **tau** is the 0.55-μm extinction optical thickness times 100 (e.g., 9 means 0.09); **IWP** is the cirrus ice-water path (g/m^2); **Deff** is the ice-particle SD effective size (μm) (again, defined as the ratio of the third to second moment of the ice-particle size distribution); and **T_Cir** is the cirrus effective temperature (K). The effective temperature is the cirrus environmental temperature at the cloud's radiative center of mass and, depending on IWP, usually lies close to the true (i.e., ice) center of mass someplace between cloud base and cloud top.

Note on the right side of Figure 4 that the balloon-observed coincident atmospheric temperature/water-vapor profile does a good job of indicating the presence of cirrus between, say, 9 and 12 km. This type of signature is evident for many (if not most) of the cirrus days at Hanscom, indicating that NWP-based water-vapor profiles might be helpful in assigning and refining cloud top/base estimates *given that the satellite data detect cloud in the first place*. In conditions where clouds are optically thicker, the satellite radiances are minimally influenced by ice particles at the lower portions of the cirrus. Augmenting the weak satellite cloud-base signal with a strong NWP water-vapor-profile signature may prove helpful in apportioning the total retrieved ice mass more accurately between cloud base and cloud top. This influences the magnitude of the retrieved IWC profile and, in turn, the extinction and particle-size profiles.

Figure 5 shows the satellite-based extinction-coefficient profile retrievals (using Eq. (28)) and the coincident lidar and radar observations for the same 29 July case shown above. Note the good agreement between the time dependence of the ground-based observations and the satellite retrievals. Figures 4 and 5 indicate that the satellite retrievals yielded results that are not in conflict with ground-based observation, which in turn helps lend credibility to our GOES-based analyses. Figure 6 contains another

sample comparison for 21 June, this time with the 35-GHz radar data. Here we also see good agreement between ground-based observation and satellite retrieval.

Figure 7 contains cloud-base/top performance summary statistics for the entire 2005 year's worth of cirrus data analysis and retrievals. For these optically thinner cirrus, cloud-height RMS values are generally less than 1 km on average.

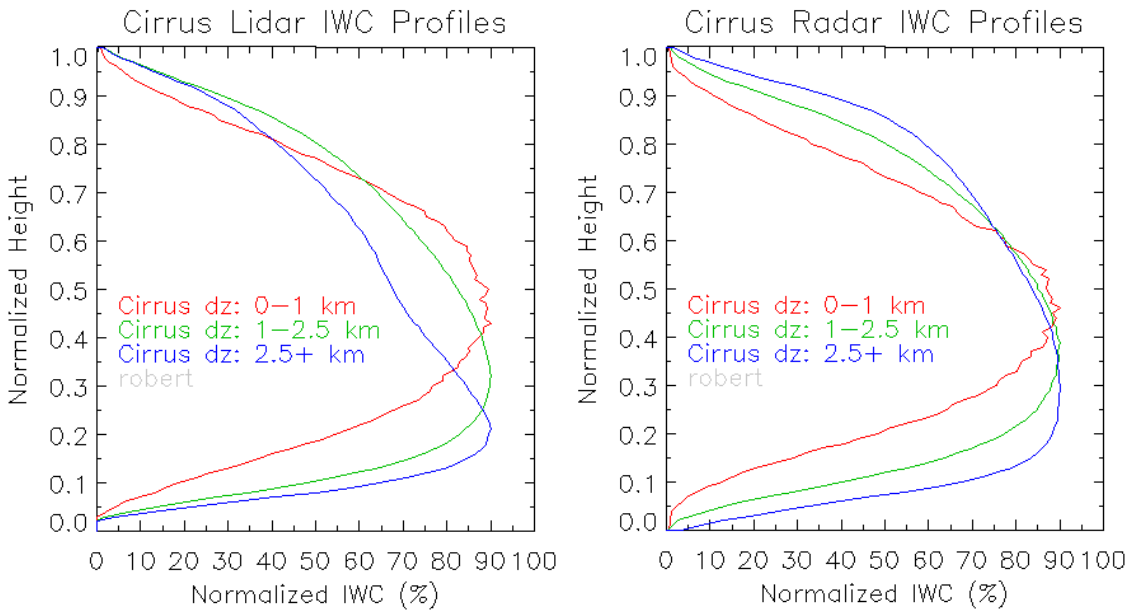

Figure 3. Plots of averaged lidar extinction (left) and radar backscatter (right) observations as a function of normalized in-cloud position for several hundred profiles between February and August 2005. Cloud base is h=0, and cloud top is h=1. These shapes are used to infer the IWC profile shape for any given GOES cirrus pixel

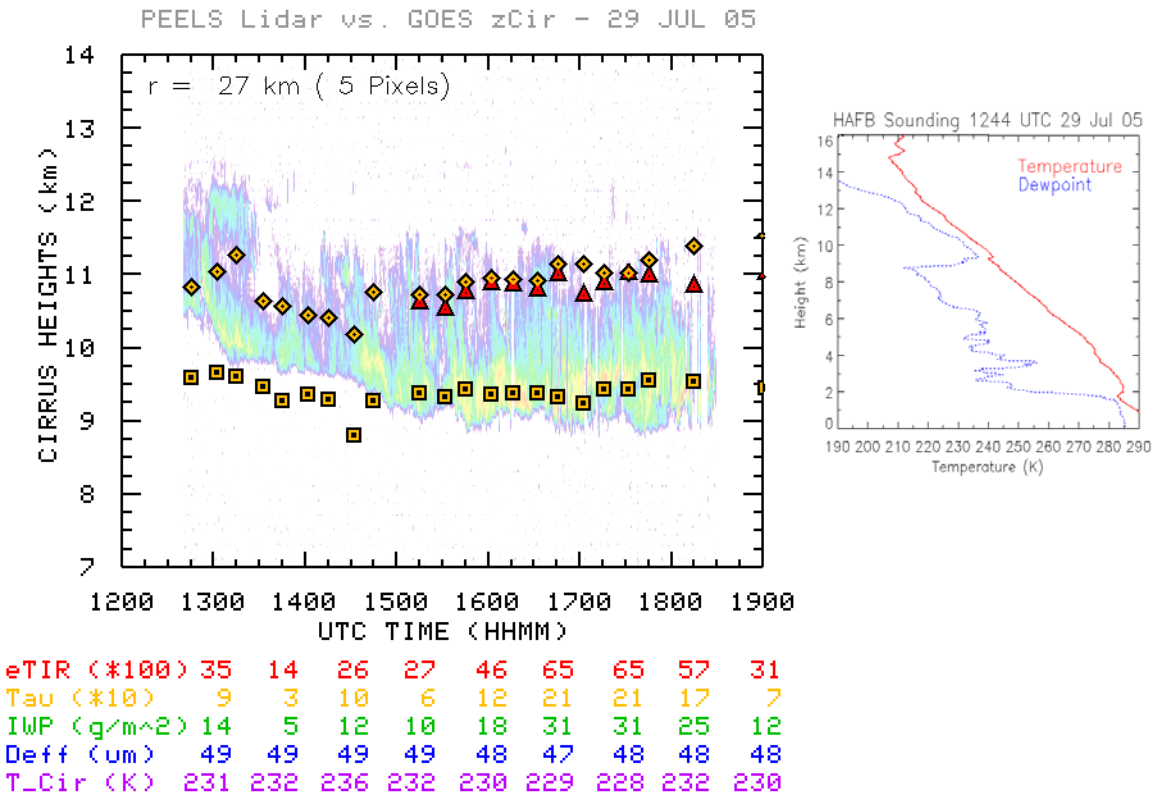

Figure 4. Comparison of GOES cloud-top and base retrievals to PEELS lidar and radiosonde for 29 Jul 05 over Hanscom AFB. Note that the water-vapor sounding does a good job in prescribing the cirrus base and, to a lesser extent, top locations

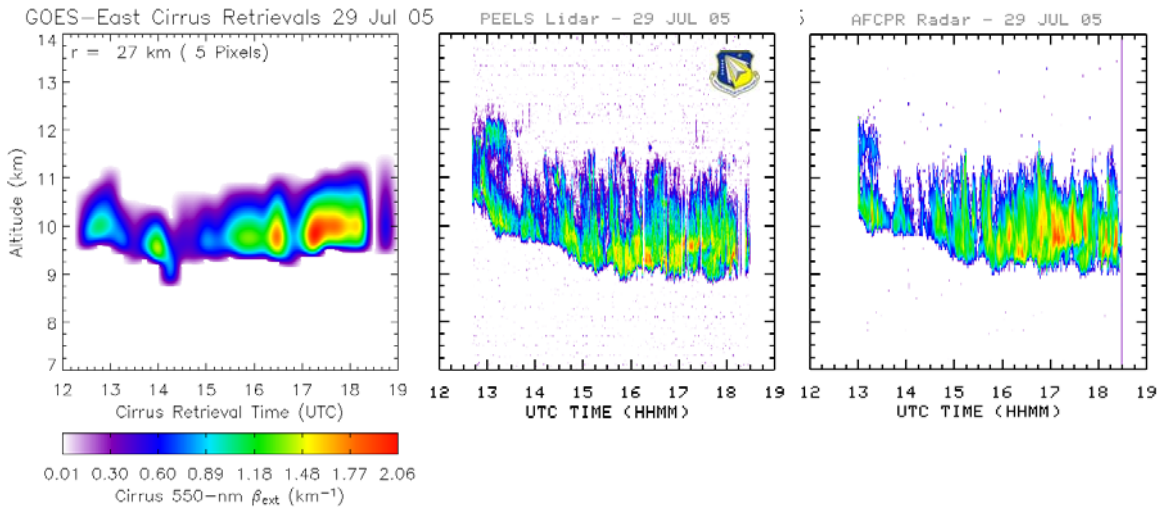

Figure 5. Comparison of satellite-derived extinction profile retrieval (left) to lidar and radar returns for 29 Jul 05 over Hanscom AFB.

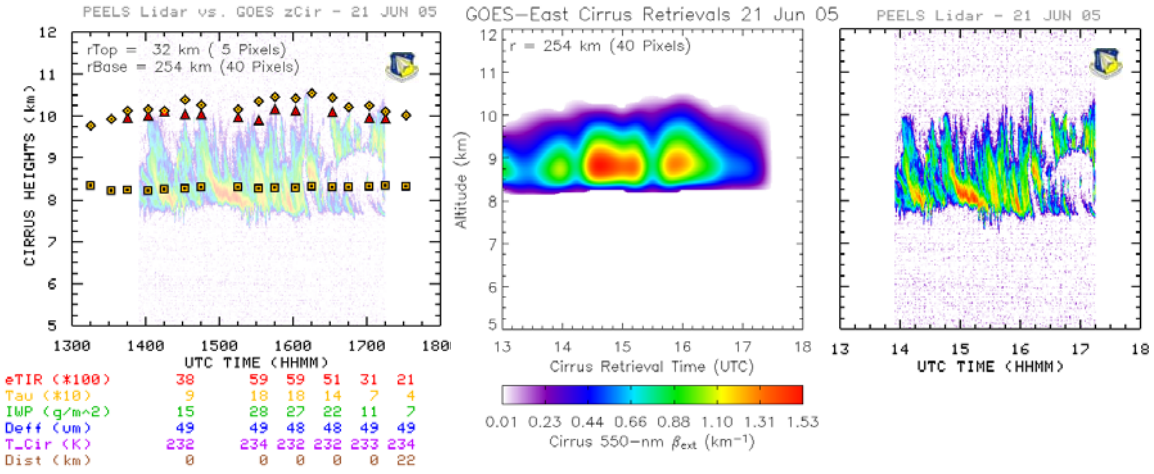

Figure 6. Comparison of satellite derived extinction profile retrieval (left) to lidar returns for 21 June 05 over Hanscom AFB.

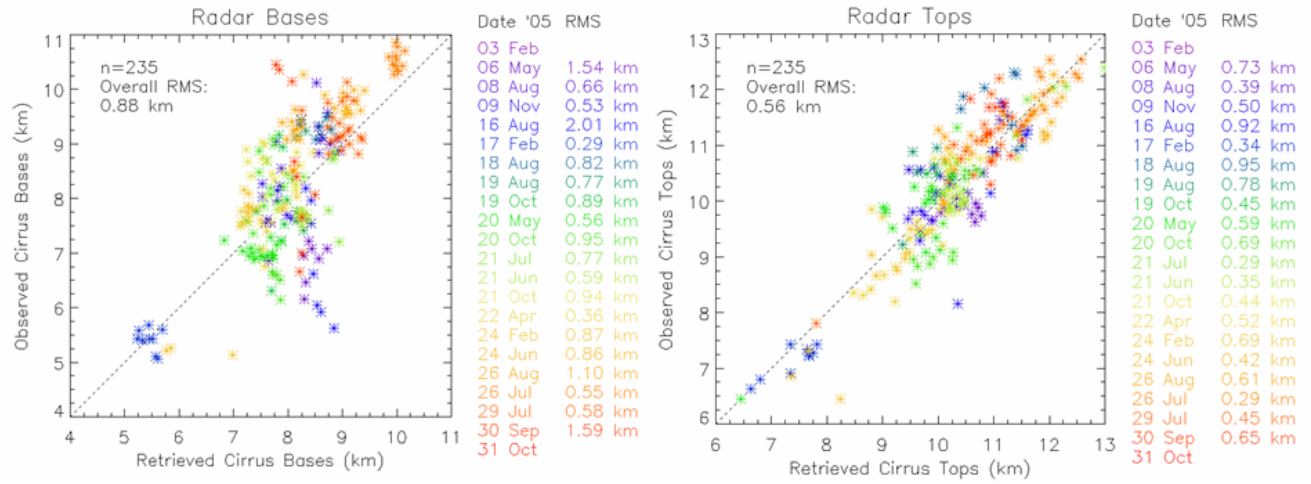

Figure 7. Comparison of cirrus cloud-base and cloud-top retrievals for the 2005 cirrus case study days. Cloud base/top "truth" was obtained using the ground-based radar observations.

7 Summary Remarks

Reasoning behind our approach to IWP and particle-size retrievals is deterministic in nature, whereas our approach to cirrus base and top is empirical. We have repeatedly observed that the local spatial variability in satellite-based cloud effective-height retrievals is observed to be a good predictor of the lidar and radar-observed cloud vertical bounds. We have found so far that the combined deterministic/empirical technique is observed to perform best for optically thinner cirrus, i.e., for cirrus through which a significant portion of the underlying surface energy is transmitted. Once the cirrus gets optically thick (TIR emissivity > 0.85 or so), cloud bases are typically overestimated because the satellite signal contains little or no information from the deeper parts of the cirrus. Nonetheless we still have a somewhat sensible estimate for cloud base that, in turn, can be used for IWC and extinction computations.

Using this approach we demonstrated our attempts at vertical profiling of extinction coefficients. Figures in Section 4 show two examples of extinction-coefficient vertical profiles retrieved using Eq. (28) along with the normalized IWC shape assumption (see Figure 3) and bulk retrievals in Table 1.

Initial comparisons of the Hanscom AFB lidar and radar data with our bulk satellite retrievals and extinction-coefficient profile estimates are very encouraging. Where these retrievals are of novel use is in their vertical mass-profiling ability. As we learn more about the distribution of ice mass throughout the cirrus depth with these and

other data sources (such as those provided more routinely by ARM), we will continue to apply that knowledge to the problem of estimating vertical profiles of ice mass, optical thickness, and particle size for climate radiative forcing and atmospheric heating-rate needs.

8 References

d'Entremont, R. P., and G. B. Gustafson, 2003: Analysis of Geostationary Satellite Imagery Using a Temporal-Differencing Technique. Earth Interactions, **7**, Paper 1.

DeSlover, D., W. L. Smith, P. K. Ppiironen, and E. W. Eloranta, 1999: A methodology for measuring cirrus cloud visible-to-infrared optical depth ratios. Journ. Atmos. Ocean, Tech., **16**, 251-262.

Heymsfield, A. J., and C. M. R. Platt, 1984: A parameterization of the particle size spectrum of ice clouds in terms of the ambient temperature and the ice water content. *Journ. Atmos. Sci.,* **41**, 846-855.

Ivanova, D., D. L. Mitchell, W. P. Arnott, and M. Poellot, 2000: A GCM parameterization of bimodal size spectra and ice-mass removal rates in mid-latitude cirrus clouds. *Atmos. Res.*, **59**, 89-113.

Ivanova, D. C., D. L. Mitchell, and G. M. McFarquhar, 2004: A trimodal size distribution parameterization for tropical cirrus clouds. *Proc. 14th ARM Sci. Team Mtg.*, 22-26 March 2004, Albuquerque. (www.arm.gov/publications/proceedings/conf14/extended_abs/ivanova-dc.pdf)

Korolev, A., G. A. Isaac, and J. Hallett, 2000: Ice particle habits in stratiform clouds. QJR Meteorol Soc., **126**, 2873-2902.

McFarquhar, G. M., and A. J. Heymsfield, 1997: Parameterization of tropical ice-crystal size distributions and implications for radiative transfer: results from CEPEX. *Journ. Atmos. Sci.*, **54**, 2187-2200.

Mitchell, D. L., R. P. d'Entremont, D. H. DeSlover and W. P. Arnott, 2003: Multispectral thermal retrievals of size distribution shape, effective size, ice water path, optical depth and photon tunneling contribution. *12th Conf. on Satellite Meteorology and Oceanography*, AMS Annual Meeting, Long Beach, California, 9-13 Feb. 2003.

Mitchell, D. L., 2002: Effective diameter in radiation transfer: General definition, applications and limitations. *J. Atmos. Sci.*, **59**, 2330-2346.

Mitchell, D. L., and A. J. Baran, 2002: Testing of the Modified Anomalous diffraction approximation with T-matrix calculations for hexagonal ice columns. *Conf. Atmos. Radiation*, Amer. Meteor. Soc., 3-7 Jun 2002, Ogden UT, J139-144.

Mitchell, D. L., W. P. Arnott, C. Schmitt, A. J. Baran, S. Haveman, and Q. Fu, 2001: Contributions of photon tunneling to extinction in laboratory-grown hexagonal columns. *Journ. Quant. Spectroscopy and Rad. Transf.*, **70**, 761-776.

Mitchell, D. L., D. Ivanova, A. Macke, and G. M. McFarquhar, 2000: A GCM Parameterization of bimodal size spectra for ice clouds. *Proc. 9th ARM Sci. Team Mtg.*, 22-26 March 1999, San Antonio. (www.arm.gov/docs/documents)

Mitchell, D. L., A. Macke, and Y. Liu, 1996: Modeling cirrus clouds. Part II: Treatment of radiative properties. *J Atmos Sci,* **53**, 2967-2988.

Twohy, C. H., A. J. Schanot, and W. A. Cooper, 1997: Measurement of condensed water content in liquid and ice clouds using an airborne counterflow virtual impactor. *J Atmos Ocean Tech*, **14**, 197-202.

Appendix A: Why are SD Shape, Ice Water Path and Effective Size Important?

Satellite-based retrievals of effective diameter (D_{EFF}) and ice water path (IWP) are needed to describe cirrus radiative properties and evaluate their influence on transmittance. Unfortunately these properties are not sufficient for describing the radiative behavior of cirrus at terrestrial wavelengths. Size distribution (SD) shape must also be known for terrestrial radiation. For example, the absorption optical depth may differ up to 44% for two cirrus size distributions having the same D_{EFF} and IWP.

Even knowing the size distribution shape is not totally sufficient for describing the radiative nature of cirrus clouds at infrared wavelengths. This is because a process called photon tunneling often contributes significantly (between 15 and 42%) to the absorption of infrared energy by cirrus ice particles, as shown in Figure A1 below. Tunneling here labels the process by which photons beyond the particle's geometric cross-section are absorbed, in comparison to absorption due strictly to the particle's geometric cross section or internal reflection/refraction. These three processes are illustrated in Figure A2. Contributions to tunneling are greatest when particle size and wavelength are comparable.

Tunneling has been parameterized for ice clouds by Mitchell and Baran (2002), whose radiation scheme was found to be accurate within 15% relative to T-matrix calculations of absorption efficiency (5% mean error) over the wavelength range 2-18 μm (see Figure A1). Additionally, mean extinction efficiency (Q_{EXT}) errors for a hexagonal-column ice cloud were ≤3% relative to measured Q_{EXT} over the same wavelength range (Mitchell, 2001). Hence it appears justifiable to use this radiation scheme, making it necessary to know the tunneling factor t_f, which ranges between 1 (for ice spheres) and 0 (no tunneling).

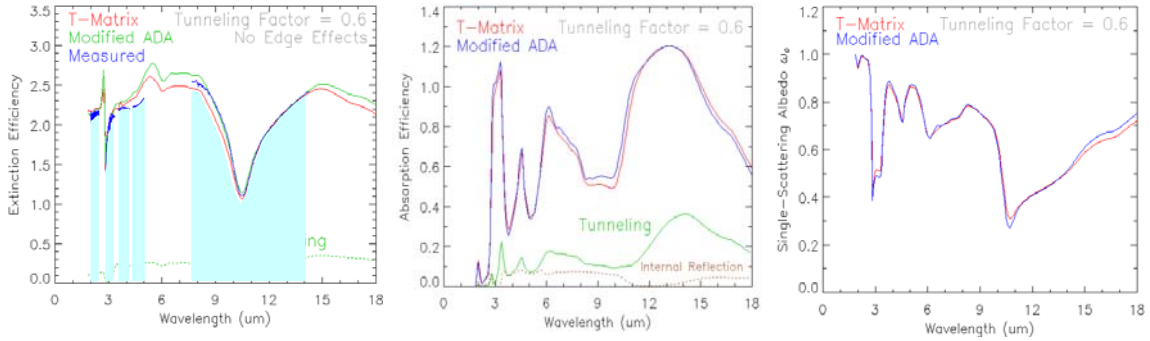

Figure A1. Plots of MADA extinction and absorption efficiencies, and single-scattering albedo, for an observed distribution of cirrus ice particles. Also plotted for comparison are T-matrix theory computations for the same SD. (See Mitchell, 2002)

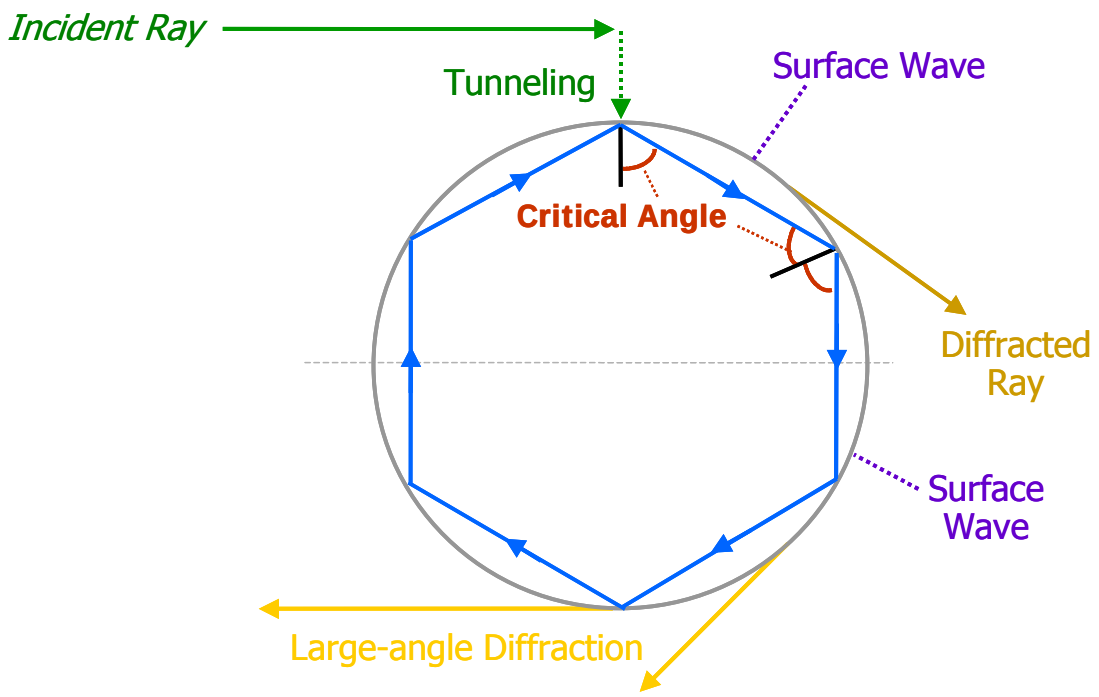

Figure A2. Depiction of the possible trajectories of an incident ray grazing a cloud particle. Photons beyond the physical cross section undergo "tunneling" into the edge domain, launching surface waves that are continually dampened as they propagate.

Appendix B: Improving Particle-Size Retrievals

As mentioned in Section 3.2.6, we have exploited a means of estimating the ice-particle effective size D_{EFF} as a function of cirrus environmental temperature. Although this assumption bears out in a time- and space-average sense, we acknowledge its shortcomings on a pixel-by-pixel basis. From the climate-forcing point of view, longwave infrared fluxes are dominated by cloud absorption optical thickness profiles. To the extent that absorption optical thickness depends on effective particle size, more accurate estimates of D_{EFF} may be required.

However, note from Eq. (20) that the direct influence of D_{EFF} on τ_{ABS} is moderated by the absorption efficiency Q_{ABS}; in other words, for infrared absorption and emission properties, absorption optical thickness is linear with IWP and the *ratio* Q_{ABS}/ D_{EFF} of absorption efficiency to effective particle size. Thus as long as the relationship between Q_{ABS} and D_{EFF} is radiatively consistent, then our retrievals of cirrus absorption properties is likely not to be suffering too much from a perhaps oversimplified parameterization between D_{EFF} and T_{CI}.

Where all of this falls apart, of course, is when scattering plays an important role in the radiation transfer. Although its influence on infrared radiances is relatively weak, scattering plays a dominant and forceful role in the scattering of sunlight at visible, near-IR, and SWIR wavelengths. This is when a more deterministic approach to retrieving D_{EFF}, and its relation with asymmetry and single-scattering albedo, is called for. To this end, we plan to incorporate the following retrieval scheme for effective particle size.

Cirrus emissivities, and hence τ_{ABS}, can be obtained spectrally from the available infrared channels of a satellite imager. In combination with a spectrum of retrieved absorption optical thicknesses, the modified anomalous diffraction theory we use for computing scattering and absorption efficiencies can be exploited to retrieve particle size. In Figure B1 it can be seen that ratios of absorption optical thickness at a given wavelength to that at 11 μm contains useful information on the effective particle size of our bimodal size distributions. From Eq. (20) it is seen that this ratio is simply the ratio $Q_{ABS}(\lambda)/ Q_{ABS}(11\ \mu m)$ since particle size and IWP are wavelength-invariant properties. This technique is similar to that outlined by DeSlover et al (1999).

The plots in Figure B1 were obtained using our MADA absorption efficiency theory outlined in Section 3.2.2, along with the bimodal mid-latitude and tropical cirrus size-distribution aircraft observations. Note hat there is a strong dependence of this ratio on particle size for most of the infrared bands available on operational meteorological satellites, including the WV and TIR bands.

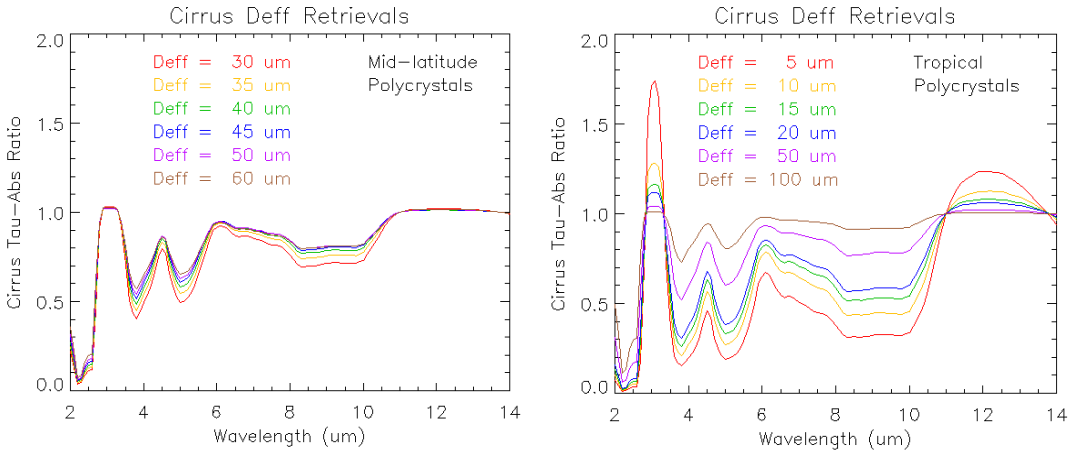

Figure B1. Plots of the absorption efficiency ratios predicted by our MADA theory as a function of effective particle size, for mid-latitude (left) and tropical (right) bimodal distributions of cirrus ice particles.

The plots show that by ratioing satellite-retrieved absorption optical thickness combinations of 3.9/11 μm or 8.55/11 μm, it is possible to retrieve D_{EFF}. These curves were generated using the ice-cloud radiation model described in Mitchell (2002), assuming N(D) for both tropical and mid-latitude cirrus, and for shapes that include rosettes, plates, hexagonal columns, and planar polycrystals. Mitchell (2002) describes that size distributions with differing D_{EFF} values can have the same radiative properties because of the behavior of the small- and large-particle modes. These curves provide insight to expected retrieval accuracies of D_{EFF}, as well as the influence of bimodal particle distributions on absorption. Size information is best obtained when using infrared bands where absorption is volume- (mass) dependent, such as at 3.9 μm. At 10.1 μm, absorption is partially mass and partially area-dependent, but is strongly area-dependent at 11.2 μm.

Global information of ice water content (IWC) in ice clouds is urgently needed for testing of global climate models (GCMs) and other applications, but satellite and ground-based retrievals of IWC and the column-integrated IWP are still in the developing stages, and tend to have large uncertainties (as high as a factor of 2 or more, depending on the radiance data used). A retrieval method is presented here that may have relatively low uncertainties, using one or more thermal channels routinely available on operational meteorological and environmental satellites.

Recent research indicates that ice cloud radiative properties depend on more than effective diameter (D_{EFF}) and ice water content (IWC). The size distribution shape, or dispersion, such as the degree of bimodality, is also an important factor at thermal wavelengths. Failure to account for this can lead to substantial retrieval errors. Hence, we have developed a retrieval scheme that accounts for the size distribution (SD) shape in mid-latitude and tropical cirrus.

For a given ice-particle shape, preliminary tests varying particle size, IWC and cloud depth, as well as accounting for surface emission and instrument noise, suggest the scheme is accurate to about ±15% over an IWP range of 1 to 100 g m^{-2}, and about ±25% over an IWP range of 100 to 200 g m^{-2}, except for very thin cirrus having unusually large crystals or multiple cloud layers. This is based on thousands of radiation transfer model retrieval simulations.

With an integrated IWP retrieval in hand, we couple it with cloud-top and cloud-base retrievals and inferences on normalized IWC-profile shapes to infer vertical profiles of cirrus radiative and microphysical properties such as the extinction coefficient and (an absolute-magnitude) IWC profile. The retrieval scheme is being tested with satellite-based retrievals and compared against in-situ radar and lidar data and from over two dozen cirrus IOPs between January and December 2005 that occurred over Hanscom AFB near Boston, Massachusetts. GOES-8 channels at 6.5 and 10.7 μm were used.